Journal of Luminescence 151 (2014) 130–137

Contents lists available at ScienceDirect

Journal of Luminescence

journal homepage: www.elsevier.com/locate/jlumin

A high sensitive ion pairing probe (the interaction of pyrenetetrasulphonate and methyl viologen): Salt and temperature dependences and applications

Jeferson Santana [a], Katia R. Perez [c], Thiago B. Pisco [a], David D. Pavanelli [a], Décio Briotto Filho [a], Daisy Rezende [a], Eduardo Rezende Triboni [d], Francisco das Chagas Alves Lima [f], Janildo Lopes Magalhães [e], Iolanda Midea Cuccovia [a], Ligia F. Gomes [b], Mário J. Politi [a,*]

[a] Departamento de Bioquímica e Departamento de Química, Instituto de Química, Universidade de São Paulo, SP, Brasil
[b] Departamento de Analises Clínicas, Faculdade de Ciências Farmacêuticas, Universidade de São Paulo, São Paulo-SP, Brasil
[c] Departamento de Biofísica, Escola Paulista de Medicina, Universidade Federal de São Paulo, São Paulo-SP, Brasil
[d] Universidade Nove de Julho, São Paulo, São Paulo-SP, Brasil
[e] Departamento de Química, Centro de Ciências da Natureza, Universidade Federal do Piauí, Centro de Ciências da Natureza, Teresina, PI, Brasil
[f] Coordenação de Química, Universidade Estadual do Piauí, Teresina-PI, Brasil

ARTICLE INFO

Article history:
Received 31 August 2013
Received in revised form
26 November 2013
Accepted 22 January 2014
Available online 19 February 2014

Keywords:
Pyrenetetrasulphonate methyl viologen
Charge transfer complex
Ion pair association
Urea effect
Vesicle characterization

ABSTRACT

The interaction between pyrenetetrasulphonate (PTS) and methyl viologen (MV^{2+}) leads to a 1:1 charge transfer complex (CTC) in the concentration range below mmol L^{-1} of the ligands. Quantum mechanical calculations show the 1:1 complex having the planar moiety of PTS and the charges of the sulfonate groups stabilized by the twisted rings of the positively charged MV^{2+} species. The peculiar nature of PTS includes high fluorescence quantum yield (~1), clear specular UV–vis spectra and fluorescence emission images, as well similar $S_2 \leftarrow S_0$ and $S_3 \leftarrow S_0$ transitions as those of $S_1 \leftarrow S_0$, all of them exhibiting well resolved vibrational structure. MV^{2+} has well known electron-accepting properties that favor the complexation. These features were studied as a function of salt concentration and temperature dependences allowing a detailed comprehension of static and dynamic association processes. Quantum mechanical calculations show the 1:1 stabilization of PTS/MV^{2+}. In addition the effect of urea on the CTC equilibrium is presented, as expected the additive acts towards the non-complexed species (solvated free ions). The fluorescence quenching of MV^{2+} over PTS highlights is one of the applications of this effect for giant vesicles characterization.

1. Introduction

Planar aromatic molecules are known to make π-interactions that can lead to molecular agglomeration as in π-stacking effects and as well in J and H aggregates [1]. Drive force for the stacking is originated from the overlap of carbon π orbitals and partial electron transfer conferring a charge transfer (CT) character to the bond. Aromatic carbon rings as pyrene, perylene and several others are candidates to present these interactions that are strong functions of solvent parameters and how the molecules are solvated [1,2].

Previous studies with a pyrene derivative (8-hydroxy-1,3,6-pyrenetrisulphonate, pyranine) (e-donor) and methyl viologen (MV^{2+}) (e-acceptor) and as well with PTS and butyl viologen showed the CT character of the ion-pairing complex formation from the appearance of new absorption bands [3]. This study also showed the participation of static and dynamic components in the fluorescence quenching of pyranine by MV^{2+} [3]. The partial electron transfer in the CT complex could be further exploited by laser flash photolysis studies where intense and large pulses promote the photoredox process [3,4].

The special spectral features of these ions as their high absorption coefficients and clear separation of the more prominent bands and as well high fluorescence yields of the pyrene derivative prompted us to pursue further with the characterization and applications of these properties.

In this study we selected a "simpler" probe the 1,3,5,8-pyrenetretasulphonate (PTS) for the absence of photoacid effects, to characterize the photophysical effects derived from the stacking

* Corresponding author.
E-mail address: mjpoliti@usp.br (M.J. Politi).

http://dx.doi.org/10.1016/j.jlumin.2014.01.062
0022-2313

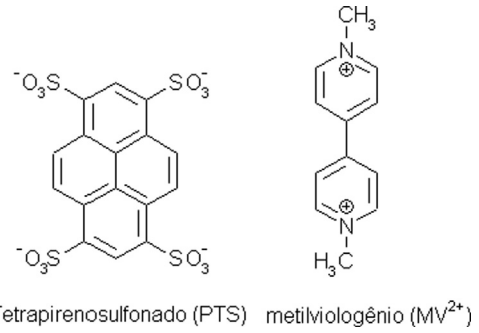

Fig. 1. Chemical structures of(please clarifiy with MC coz check instruction) betetrapyrenesulphonate (PTS) and methyl viologen (MV^{2+}).

(dimer) formation with MV^{2+}. As PTS and MV^{2+} (Fig. 1) are soluble in water and have opposite charges the screening effect of salts is also investigated. From spectrophotometric and fluorimetric determinations, ground and excited states dimer formation is observed. The effect of urea on the ion pairing destabilization is also highlighted [5]. To demonstrate one of the pair formation applications the effect on vesicles characterization is also highlighted.

2. Materials and methods

2.1. Materials

Pyrenetetrasulphonate (Sodium salt, Eastman Kodak) (PTS) was used as received due to the absence of detectable impurities on TLC plates [3]. Methyl viologen (MV^{2+}) (Aldrich) was recrystallized twice from cold acetone/methanol (85/15 v/v). Stock solutions of these compounds were freshly prepared and kept refrigerated in dark. Urea (Carlo Erba) was recrystallized from hot ethanol; 6 mol L^{-1} solutions gave an electrical conductivity of 18 μS showing the lack of ionic contaminants. Electrolyte solutions were prepared from well dried solids from the best analytical available salts. Water was doubly distilled and further purified and deionized with a Mill-Q system.

2.1.1. Quantum mechanical calculations

Molecular dynamics calculations have been performed with the Gaussian 09 package [14]. The molecular geometry optimizations of the PTS, viologen and complex (PTS/MV^{2+}) were performed using the Kohn–Sham density functional theory (DFT) [15] with the Becke three-parameter hybrid exchange–correlation functional known as B3LYP [16,17] along with the basis set 6-31G(d) [18]. Vibrational frequencies were calculated from analytic second derivatives to check the minimum on the potential energy surface. Zero-point vibrational energies were added on the basis of B3LYP frequency calculation (uncalled) using the same basis set as for the geometry optimizations. The polarizable continuum model (PCM) [19] is employed to optimize the structures in a cavity created via a series of overlapping spheres simulating the water solvation. The PCM is based on a description of the solvent as macroscopic continuum medium having suitable properties (dielectric constant, thermal expansion coefficient, *etc.*). In this procedure, the solute is embedded in a cavity in the dielectric medium and the solute–solvent interactions are described in terms of the reaction field due to the presence of the dielectric medium, which acts as perturbation on the Hamiltonian of the solute through its reaction potential [19].

2.2. Giant vesicles preparation

The phospholipid 1,2-dioleoyl-sn-glycero-3-phosphatidylcholine (DOPC, Avanti Polar Lipids) was used without further purification. Sucrose and glucose (SigmaAldrich). GUVs were obswerved in a 100 uL cuvette. Typically, Giant Unilamellar Vesicles (GUVs) were formed in a solution containing 5×10^{-3} mol L^{-1} PTS. For monitoring, an aliquot of 50 μL of the vesicle suspension was mixed with the same volume of a solution containing 5×10^{-3} mol L^{-1} MV^{2+}. MV^{2+} suppresses PTS fluorescence outside vesicles. Once PTS, MV^{2+} and PTS/MV complexes do not permeate through the bilayer permeable observed fluorescence arises from free unquenched PTS [6].

GUVs of DOPC were generated using the electroformation method [7] between two parallels Pt electrodes in a Teflon custom chamber. The chamber consists of a block of Teflon with a slot sufficiently large to submerge the two electrodes in the formation medium with a 1 mm gap in between. Before use, the Teflon chamber and the electrodes are thoroughly cleaned with solvents and copious amounts of deionized water.

Briefly, 5 μL of a 1 mg mL^{-1} lipid chloroform solution was spread in the electrodes. The lipid film in the electrodes is left to dry in a vacuum chamber for 2 h to remove all traces of the organic solvent. The chamber was filled with 0.1 mol L^{-1} sucrose solution having PTS 5×10^{-3} mol L^{-1}. The electrodes were connected to a sinusoidal function generator and an AC current of 3 V with a 10 Hz frequency was applied for 2 h. The vesicle suspension was transferred to an Eppendorf tube.

GUVs were observed in a 100 μL fluorescence cuvette, extensively washed before experiments. Typically, 50 μL of vesicle suspension was mixed with an equal volume of 0.1 mol L^{-1} glucose solution creating a sugar asymmetry between GUVs interior and exterior. Density gradient causes vesicles to sediment in the observing chamber for easy observation, while refraction

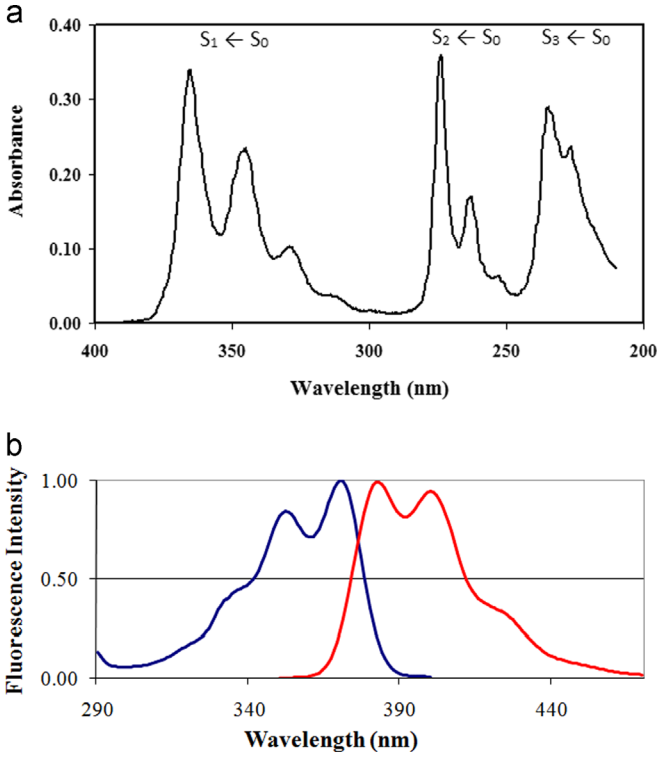

Fig. 2. (a) UV–vis spectrum of [PTS] = 1×10^{-5} mol L^{-1} in H_2O. (b) Normalized uncorrected fluorescence spectra of [PTS] = 1×10^{-5} mol L^{-1} in H_2O, excitation spectra (λ_{em} = 430 nm), and emission spectra (λ_{ex} = 365 nm) (excitation and emission slits = 10 mm, T = 25 °C).

index gradient enhances contrast through phase-contrast monitoring. The osmolarities of the sucrose and glucose solutions were measured with a cryoscopic osmometer (Advanced Instruments Osmometer, Model 3250) and carefully matched to avoid osmotic pressure effects.

GUVs were monitored by phase-contrast and/or fluorescence microscopy in an inverted microscope Eclipse TS100F (Nikon). Images were digitalized by a CCD camera LE-D (Nikon) and analyzed with the Scion Image software (Scion Corporation, free software). A UV-2A block filter (Nikon) was used in monitoring PTS fluorescence (excitation between 340 and 380 nm and emission >420 nm).

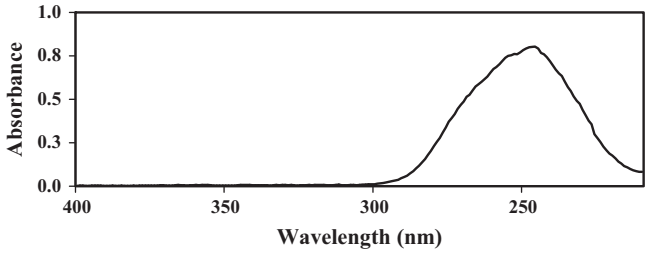

Fig. 3. UV–vis spectrum of $[MV^{2+}]=3{,}85\times10^{-5}$ mol L^{-1} in H_2O.

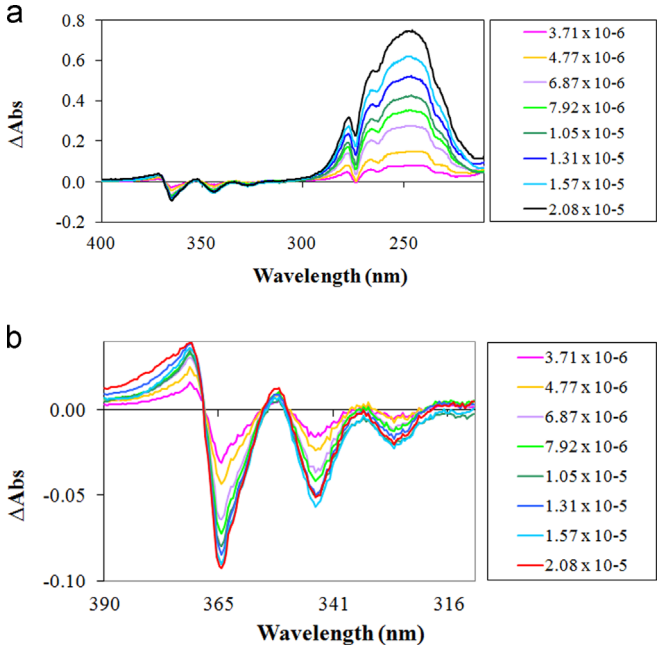

Fig. 4. (a) Difference spectra (ΔAbs) of $[PTS]=1\times10^{-5}$ mol L^{-1} with the addition of $[MV^{2+}]$ (from top to bottom at $\lambda=250$ nm)=2.08, 1.57, 1.31, 1.05, 0.792, 0.687, 0.477, and 0.371×10^{-5} mol L^{-1} in the presence of 0.05 mol L^{-1} NaCl. In these assays [PTS] is kept constant. (b) Spectra amplification from 390 nm to 310 nm.

3. Results and discussion

3.1. PTS, MV^{2+} and PTS/MV^{2+} spectral data

In Figs. 2 and 3 the UV–vis absorption spectra of PTS and of MV^{2+} in H_2O are presented. PTS presents a S_0–S_1 transition starting at 380 nm and extending to 310 nm, typical vibration bands peaking at 365, 346, 330 and 311 nm (extinction coefficients for these transitions are ~34,000, 24,000, 10,000 and 3500 mol L^{-1} cm^{-1}, respectively) are observed. These bands correspond to a ΔE spacing of $\sim1.49\times10^{-4}$ nm^{-1} that corresponds to 4.2 kcal mol^{-1}. The PTS although having four sulfonate groups, the pyrene moiety is hidden from water contact given the observed vibrational structure in the electronic transition spectra. Following S_0–S_2 and S_0–S_3 transitions peaking at 260 and 220 nm regions is observed. These bands also present vibrational structure and reflect the rigid structure of excited states of PTS. In Fig. 2B the fluorescence emission spectra are presented and a typical mirror image is observed, once again showing the water hating characteristic of the chromophoric moiety of PTS. Fluorescence yield of PTS is almost unitary [8] and associated with its lifetime ~11 ns confers its good properties for fluorimetric analysis [8,9].

Absorption spectra of MV^{2+} on the other hand are almost featureless (Fig. 3); the band shows a peak at 247 nm and a small shoulder 10 nm before, extinction of the peak is ~20,400 M^{-1} cm^{-1} in agreement with literature values [10,11]. These properties added to those of PTS allow their use in the regime of low concentrations, a good adjective for medium probes. Addition of MV^{2+} over a constant PTS concentration results in several changes easier to be detected by the spectra difference (ΔAbs) shown in Fig. 4. As observed with pyranine [3] or cyclotetrachloromotropylene [12] and MV^{2+} a new transition centered at 380 nm grows up. This band is assigned to a charge transfer (CT) from PTS to MV^{2+} (as those at 410 and 620 nm related in Refs. [3,12]). From these data and by numerical fitting according to an interaction model, an association constant can be derived; however determining the interaction stoichiometry results in a proper analysis.

3.2. PTS/MV^{2+} complex stoichiometry

In Fig. 5 a typical result for PTS/MV^{2+} complexation stoichiometry determination is depicted. In this method, known as the continuous variation [13], the sum of PTS and MV^{2+} species is kept fixed but the individual concentrations vary. As can be noticed in Fig. 5 the spectra of PTS and MV^{2+} are well defined and as the concentration of one of them decreases the other increases. From these experiments and the known spectral values for samples having only PTS (in Table 1, a calculation example is presented), the determinations of the unbound fractions are straightforward.

A series of experiment were conducted within the limit of "low" total PTS/MV^{2+} and with the several constraints studied (salt, urea)

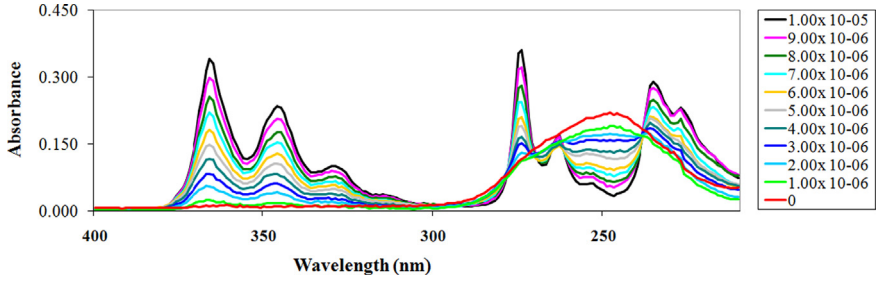

Fig. 5. Complexation stoichiometry determination in the presence of 0.05 mol L^{-1} NaCl. Total {[PTS]+[MV^{2+}]} are 1.00×10^{-5} mol L^{-1}. From top to bottom at $\lambda=365$ nm. MV^{2+} concentrations are 0.0, 1.00×10^{-6}, 2.00×10^{-6}, 3.00×10^{-6}, 4.00×10^{-6}, 5.00×10^{-6}, 6.00×10^{-6}, 7.00×10^{-6}, 8.00×10^{-6}, 9.00×10^{-6}, and 10.00×10^{-6} mol L^{-1}.

Table 1
Continuous variation method for PTS–MV^{2+} complex stoichiometry determination.

	PTS uncomplexed fraction										
	1	**0.9**	**0.8**	**0.7**	**0.6**	**0.5**	**0.4**	**0.3**	**0.2**	**0.1**	**0**
Abs at 346 nm	0.235	0.207	0.177	0.153	0.128	0.106	0.083	0.063	0.042	0.018	0.011
Abs difference compared to unbound PTS	0.000	0.028	0.058	0.082	0.107	0.128	0.152	0.172	0.193	0.216	0.224
Fraction *x* in the ABS difference	0.000	0.025	0.046	0.057	0.064	0.064	0.061	0.052	0.039	0.022	0.000

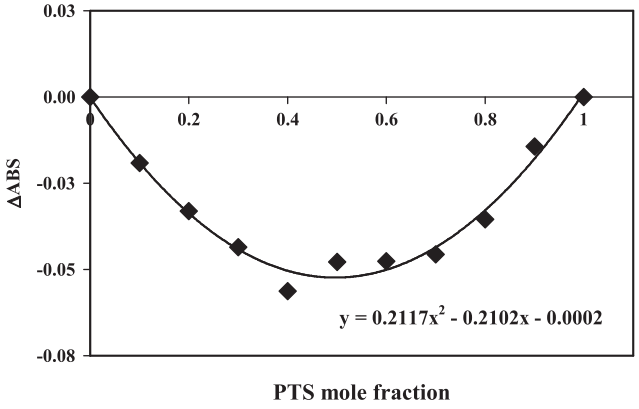

Fig. 6. ΔAbs *vs.* PTS mole fraction from data in Fig. 5 and in Table 1. Second order equation fit.

all of them gave the same parabolic profile as exemplified in Fig. 6. From the second-degree equation the abscissa minimal (Abs_{min}) is found and from its value the searched stoichiometry is calculated. Within the conditions used the Abs_{min} values were −0.5 which resulted in a 1:1 stoichiometry, valid for low PTS/MV^{2+} concentrations ([PTS]$\sim 10^{-5}$ mol L^{-1}). From the known stoichiometry values of the complexation constant (K_S) were calculated from the absorption difference (Fig. 4) at various salt concentrations. These values are summarized in Table 2.

3.3. *Molecular dynamics of PTS/MV^{2+} complex*

Molecular dynamics calculations for a 1:1 PTS/MV^{2+} complex are presented in Fig. 7. A good matching of PTS sulfonate group with the distorted rings of MV^{2+} (see Section 2) can be observed. After a complete geometry optimization of the PTS, MV^{2+} and PTS/MV^{2+} the interaction energy was obtained as the total energy difference between the PTS, MV^{2+} and the complexes as follows:

$$E_{INT} = E_{COMPLEX} - (E_{PTS} + E^{2+}_{MV}) \quad (1)$$

The counterpoise corrections have been applied to calculate the binding energies in order to account for basis set superposition errors (BSSE) [20]. Calculations results are summarized in Table 4. Data show the large enthalpic contribution due to the electrostatic interaction PTS/MV^{2+} either with corrections or not. Data compared to the experimental values are however over estimated (see Section 3.4).

3.4. *PTS/MV^{2+} complex emission properties*

A typical fluorescence suppression data of PTS by MV^{2+} is presented in Fig. 8. The ratio of the fluorescence intensities in the absence (I_o) and presence (I) of the suppressor (Stern–Volmer plot) is presented in the inset of Fig. 8. Clearly an upward curvature is observed indicating the occurrence of static (K_S) and dynamic (K_D) suppression processes. Data linearization via $[(I_o/I)-1]/[S]$ or equivalently by a second order fit via $\{(1+K_S[S])(1+K_D[S]\}$, where

Table 2
Ground state complexation constants (K_S) as functions of salt and temperature.

[NaCl] mM	K_S (25)	K_S (30)	K_S (35)	K_S (40)
0	5.74×10^4	7.54×10^4	5.56×10^4	4.51×10^4
25	1.25×10^4	1.09×10^4	1.19×10^4	8.56×10^3
50	7.48×10^3	5.66×10^3	5.81×10^3	4.98×10^3
100	3.59×10^3	2.58×10^3	2.53×10^3	4.50×10^3
150	1.90×10^3	1.84×10^3	1.88×10^3	1.71×10^3
300	1.08×10^3	1.36×10^3	1.12×10^3	881
Limiting values[a]	4.38×10^4	4.18×10^4	3.80×10^4	3.27×10^4

[a] Limiting values are obtained from Ln K_S *vs.* SQRT {[Salt]} plots; see Fig. 10.

S is the suppressor agent, confirmed the participation of both static and dynamic mechanisms. A complete analysis including salt dependences and temperature is depicted in Fig. 9 and Tables 2 and 3. In Fig. 9, a decrease in the upward curvature with the increase in salt concentration is observed indicating that in high salt $\sim$0.300 mol L^{-1} the static (K_S) mechanism is predominant. In Tables 2 and 3 the temperature effect over K_S and K_D (see below) shows a small influence but clearly K_S is higher than K_D. It is necessary to notice that values presented in Tables 2 and 3 are a mean of at least 5 independent measurements. Discrepancies in specific mean values with temperature and low ionic strength are observed from experimental errors (see for example, row 1 in Tables 2 and 3). It is important to notice again that the constants K_S and K_D are calculated from a second order equation fit using the fluorescence suppression data or equivalently by the linear fit of the suppression data over the suppressor concentration *vs.* the suppressor concentration (see Eq. (1)). This data manipulation results in large error propagation and further examination of a typical data, as presented in Fig. 9, shows that increasing the ionic strength from 0.025 to 0.300 mol L^{-1} the suppression goes from a straight line to curved and again straight line. As commented above the suppression at low salt is static and dynamic and as the ionic strength increases the dynamic and static components merge toward the same values. As mentioned the dynamic term is lower than the static one, also the temperature dependences of both constants are low; accordingly data in Tables 2 and 3 are important to unravel the suppression mechanisms. Overall trends show the correctness of calculations.

From these sets of values (ΔAbs, fluorescence suppression, and so on), the static and dynamic complexation constants were obtained as functions of salt and temperature. Tables 2 and 3 summarize the arithmetic mean values for K_S and K_D. Once again, K_S are about six times larger than the dynamic (K_D) ones. Clearly as the ionic strength increases with the reduction in the long-range attractive electrostatic potential, K_S approaches K_D values. In parallel the curvature observed in the Stern–Volmer plots also decreases (Fig. 9). In Fig. 9 data from Tables 2 and 3 are presented for better effect visualization. Reasonable liner dependence with square root of salt concentration is observed. Limiting K_S (K^0_S) and K_D (K^0_D) values are presented in last row in Tables 2 and 3; these values are calculated by taking the natural logarithm *vs.* the square root of salt concentration (Fig. 10).

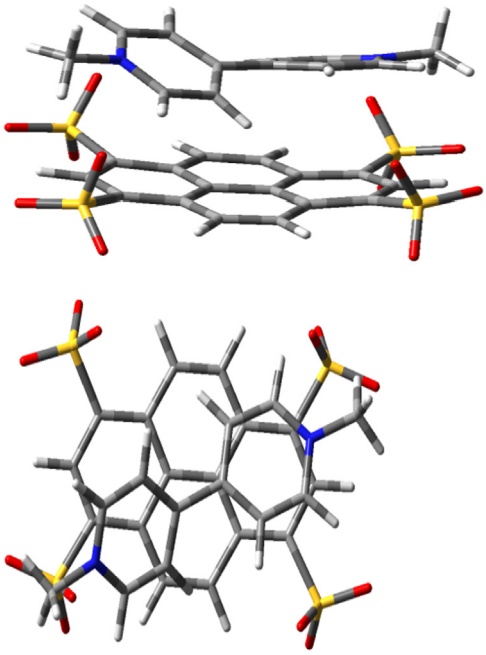

Fig. 7. PTS/MV^{2+} 1:1 complex molecular model.

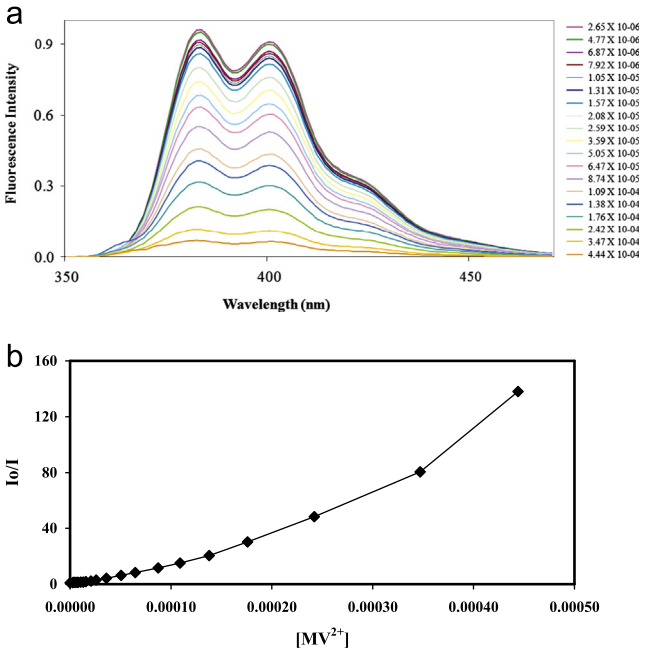

Fig. 8. Normalized fluorescence intensity of [PTS]$=1\times10^{-5}$ mol L^{-1} as a function of MV^{2+} addition in the presence of 0.05 mol L^{-1} [NaCl] (from top to bottom [MV^{2+}]$=0.00$, 2.65×10^{-6}, 4.77×10^{-6}, 6.87×10^{-6}, 7.92×10^{-6}, 1.05×10^{-5}, 1.31×10^{-5}, 1.57×10^{-5}, 2.08×10^{-5}, 2.59×10^{-5}, 3.59×10^{-5}, 5.05×10^{-5}, 6.47×10^{-5}, 8.74×10^{-5}, 1.09×10^{-4}, 1.38×10^{-4}, 1.76×10^{-4}, 2.42×10^{-4}, 3.47×10^{-4}, and 4.44×10^{-4} mol L^{-1}). Inset I_o/I *vs.* [MV^{2+}].

From the temperature dependence on K_S^0 and K_D^0, ΔH_S, ΔS_S, ΔH_D, and ΔS_D calculated are, respectively, -8.15 kJ/mol, 61.6 J (° mol^{-1}), -15.89 kJ mol^{-1}, and 29.92 J (° mol^{-1}) (Fig. 11). These values result in ΔG_S^0 and $\Delta G_D{}^0$ at 25 °C of -26.51 and -24.59 kJ mol^{-1} at 25 °C, respectively. These values point to the favorable enthalpic interaction as well the gain in entropy from the changes in solvations of MV^{2+} and PTS from separated ions to the geminated pair. Solvated ions have structured water molecules in their closest surround, upon geminate pair formation some of these molecules are released which increases the entropic factor (see Ref. [21]).

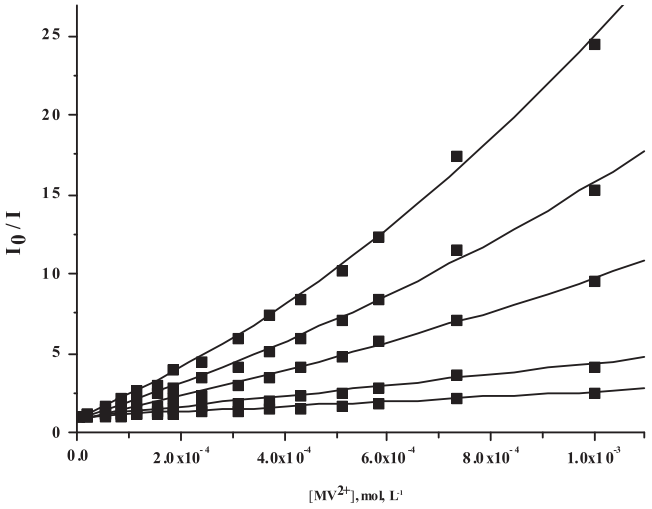

Fig. 9. Salt effect on the fluorescence intensity ratio (I_o/I) measured at 385 nm as a function of [MV^{2+}] at 25 °C. Salt concentrations are indicated in the figure.

Table 3
Excited state complexation constants (K_D) as functions of salt and temperature.

[NaCl] mM	K_D (25)	K_D (30)	K_D (35)	K_D (40)
0	2.37×10^4	8.58×10^3	2.95×10^4	1.43×10^4
25	2.60×10^3	3.07×10^3	2.3×10^3	1.3×10^3
50	1.53×10^3	2.27×10^3	1.14×10^3	775
100	696	785	972	305
150	941	285	176	576
300	383	229	533.5	450
Limiting values[a]	1.54×10^4	1.08×10^4	9.41×10^3	8.53×10^3

[a] Limiting values are obtained from Ln K_S *vs.* SQRT {[Salt]} plots; see Fig. 10.

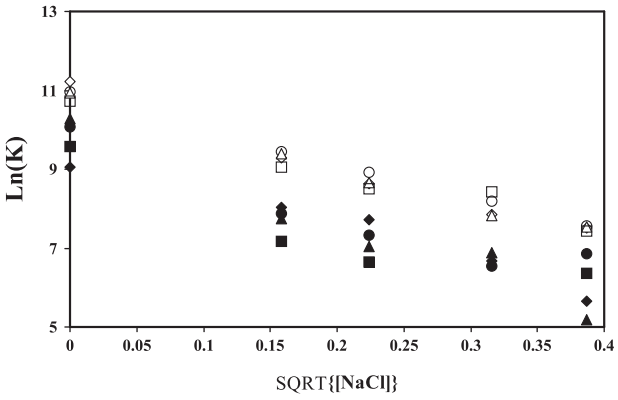

Fig. 10. Ln(K_S) (open symbols) and Ln(K_D) (full symbols) as a function of the SQRT {[NaCl]} at 25 °C (○), 30 °C (◇), 35 °C (□), 40 °C (△) and 25 °C (●), 30 °C (◆), 35 °C (▲), 40 °C (■). See Table 2 (K_S) and Table 3 (K_D) for values.

Calculated ΔH (Table 4) are clearly overestimated once the model is solvent featureless. The main point with these calculations is to derive a molecular picture of the PTS/MV^{2+} complex respecting bond angles, atoms distances and else. Calculations show also the high contribution of the electrostatic character of the interaction.

3.5. *Effect of urea on the PTS/MV^{2+} ion pair*

Giving the ionic general features of PTS/MV^{2+} interaction the effect of urea concentration on the complex formation is investigated. Using 1×10^{-5} mol L^{-1} PTS and 6.4×10^{-6} mol L^{-1} MV^{2+} in the presence of 0.05 mol L^{-1} NaCl and the absence at $T=298$ K

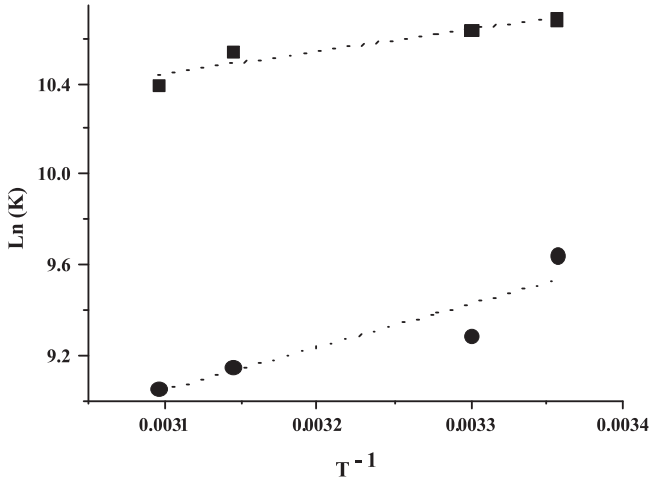

Fig. 11. Arrhenius plot for $Ln(K_S^0)$ (■) and $Ln(K_D^0)$ (•) against T^{-1}.

Table 4
Interaction energy in vacuum and water.

Vacuum[a]	Water[a]	Vacuum[b]	Water[b]
−705	−740	−690	−715

[a] without BSSE (in kJ mol^{-1}).
[b] with BSSE (in kJ mol^{-1}).

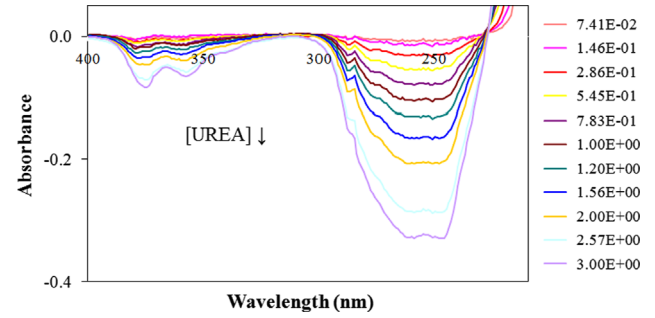

Fig. 12. ΔAbs *vs.*[urea] for PTS ([PTS] = 1×10^{-5} M) in the presence of MV^{2+} ([MV^{2+}] = 6.4×10^{-6} mol L^{-1}) and 0.05 mol L^{-1} NaCl at T=25 °C in the presence (top to bottom) of 7.41×10^{-2}, 1.46×10^{-1}, 2.86×10^{-1}, 4.19×10^{-1}, 5.45×10^{-1}, 7.83×10^{-1}, 1.00, 1.20, 1.56, 2.00, 2.57 and 3.00 mol L^{-1} of urea.

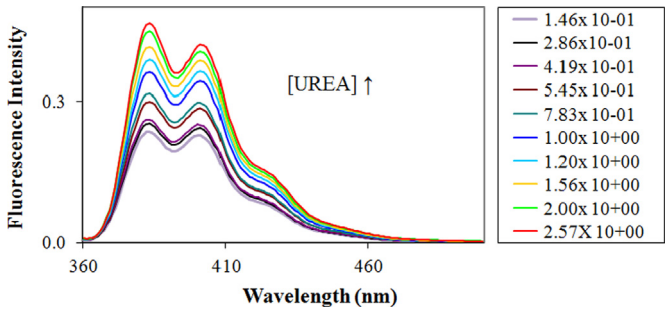

Fig. 13. Fluorescence intensity of PTS ([PTS] = 1×10^{-5} mol L^{-1}) in the presence of MV^{2+} ([MV^{2+}] = 6.4×10^{-6} mol L^{-1}) at T=25 °C in the presence (bottom to top) of 0.00, 7.41×10^{-2}, 1.46×10^{-1}, 2.86×10^{-1}, 4.19×10^{-1}, 5.45×10^{-1}, 7.83×10^{-1}, 1.00, 1.20, 1.56, 2.00, and 2.57 mol L^{-1} of urea.

the effect of urea on K_S (observed by the decrease in the absorbance difference ΔA) and on K_S and K_D (observed by the de-quenching process) is presented in Figs. 12 and 13, respectively. In both types of experiments urea affects the geminated ion pair, favoring the free ions. Accordingly a decrease in ΔA arises from the augment in free PTS and in free MV^{2+} given that the first spectrum is taken as the reference and zeroed. In parallel the fluorescence augments once the free PTS is favored. Both signals (ΔA and ΔF) seem to level of above 4 mol L^{-1} urea; it should be recalled however that the experimental conditions are distinct in data presented in Figs. 12 and 13 to point out the apparent data difference. In conclusion the urea effect affects the geminate pair (complex) formation both in the ground and excited states. Urea–water solutions being understood as a more polar media than water [5] indicate according to this argument that the drive force is enthalpic in favor of the separated ions, once in principle the entropic factor would be the same in both cases. Experiments are being conducted to exploit in detail the thermodynamics features of the complex formation and shall be presented in the due time.

In order to get a hint on the time basis of the urea effect, a thermal reaction among opposite ions was investigated. The elected reaction is the Alkaline Hydrolysis of 4-*N*-butyl-cyanopyridinium (BCP) a well documented reaction [22] that show pH and product composition dependence easy to follow in a simple spectrophotometer. The reactant was prepared as before, recrystallized and properly dried. Data showed the absence of urea effects in the range between 0 and 5 mol L^{-1} urea, in both the reaction rate constants and in the product distribution (data not presented). These results show that the effect of urea, as a "better" water by the increase in the dielectric medium constant, leads to the diminishing in ion pairing processes, occurs in a time frame under nanoseconds and not in the millisecond where BCP/OH^- associates to undergo the hydrolytic reaction. This reasoning is in accordance with the general understanding that processes involving water and urea molecules, as solvation, rotation and so on are very rapid [23].

3.6. *Application example of PTS/MV^{2+} complex for giant vesicle characterization*

Finally to present a simple application of PTS/MV^{2+} association, we present a vesicle characterization using the probes PTS and MV^{2+}. In Fig. 14 the fluorescence decay of PTS entrapped in GUV (see Section 2) due to the complexation with MV^{2+} is presented. At the beginning of experiment non-entrapped PTS is quenched by externally added MV^{2+}; observed fluorescence is from non-complexed PTS inside vesicles. In the absence of MV^{2+} the fluorescence signal is constant within 30–50 min observation (data not shown). It can be observed that within the time frame of the assay (~11 min) the GUV is still intact (see last frame in Fig. 14) but the blue emission (PTS) decays[1] [24]. This decrease is assigned to the bilayer palisade leakage by pore formation that leads to the MV^{2+} influx and PTS efflux from the GUV and formation of PTS/MV^{2+} [25]. For the present work data in Fig. 14 is only to highlight potential applications of the PTS/MV^{2+} features; full detail of PTS/MV^{2+} applications is under preparation. The effect of charged particles as CTABr or SDS micelles over either PTS or MV^{2+} and the complex species can be easily estimated as observed with pyranine and MV^{2+} [3].

4. Conclusion

The interaction of PTS with MV^{2+} yielding a 1:1 complex is studied in detail. Ground state and excited state equilibria show a highly favorable ΔG_o with contributions of both enthalpic and entropic terms. The geminate pair formation is affected by the

[1] A detailed microscopy study using GUVs, PTS and MV2+ is being prepared.

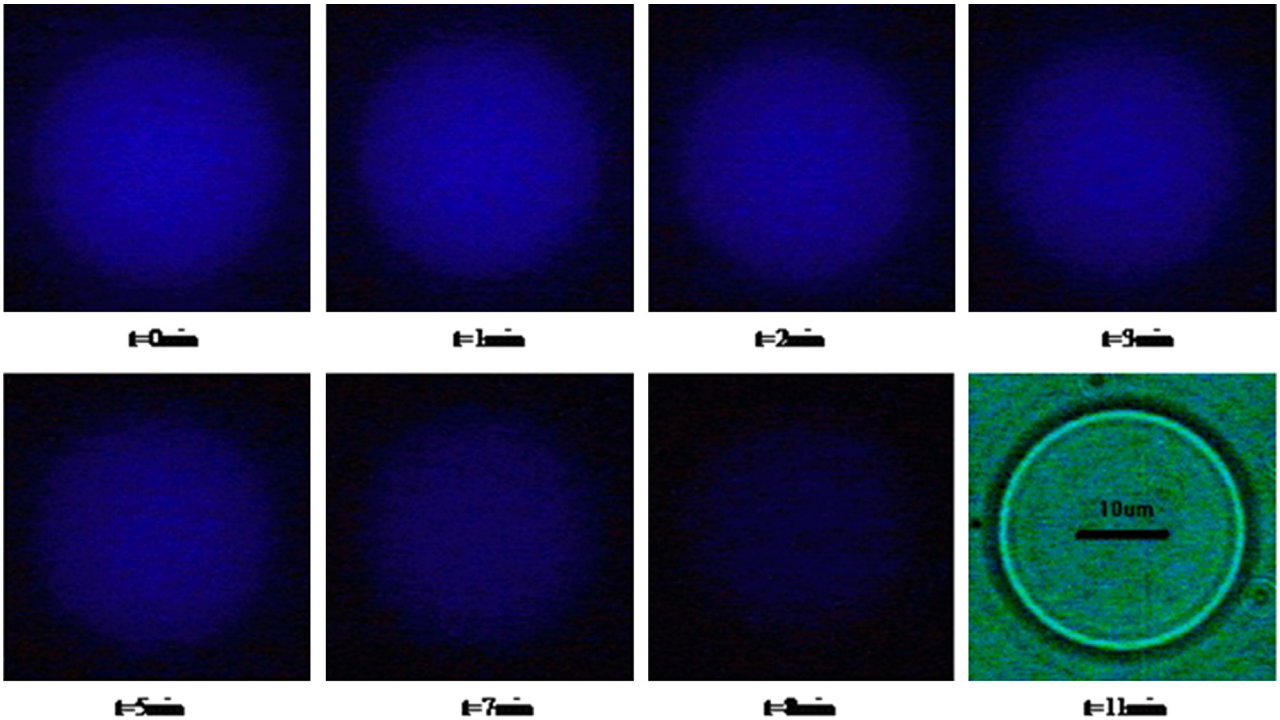

Fig. 14. Fluorescence decay of PTS entrapped in GUV by complexation with MV^{2+}. Notice that after 11 min observation the GUV is still time intact. Fiducial bar is indicated in the figure last frame.

action of urea that by increasing the medium polarity stabilizes the solvated separated ions. An effect assigned to the increase in the dielectric constant affects the stabilization in the charges. Microscopic study with GUV highlights one application of the complex formation and the fluorescence high emission yields of PTS for colloids studies.

Acknowledgments

We wish to express our sincere gratitude to the Graduate School of the Chemistry Institute (USP) for a fellowship to Dr. Larry Romsted from the Department of Chemical Biology, Rutgers University, USA for lecturing a course on Colloids and to all students enrolled for making some of the initial experiments and to the granting agencies CAPES, CNPQ, and FAPESP for their continuous efforts in Science Development.

References

[1] Wei Wang, LiQiong Wang, Bruce J. Palmer, Gregory J. Exarhos, Alexander D.Q. Li, J. Am. Chem. Soc. 128 (2006) 11150.
[2] Yang Liu, Yongjun Li, Li Jiang, Haiyang Gan, Huibiao Liu, Yuliang Li, Junpeng Zhuang, Fushen Lu, Daoben Zhu, J. Org. Chem. 69 (2004) 9049.
[3] E.B. De Borba, C.L.C. Amaral, M.J. Politi, R. Villalobos, M.S. Baptista, Langmuir 16 (2000) 5900;
K. Kano, J.H. Fendler, Biochem. Biophys. Acta 509 (1978) 289;
W. Yu, X.-Y. Wang, J. Li, Z.-T. Li, Y.-K. Yan, W. Wang, J. Pei, Chem. Commun. 49 (2013) 54.
[4] M. Gutman, E. Nachliel, R. Friedman, Photochem. Photobiol. Sci. 5 (2006) 531;
A.B. Kotlyar, N. Borokov, S. Kiryati, E. Nachliel, M. Gutman, Biochemistry 33 (1994) 873;
A.B. Kotlyar, N. Borokov, S. Raviv, L. Zimanyl, M. Gutman, Photochem. Photobiol. 63 (1996) 448.
[5] Mario J., Politi; HernanChaimovich; Iolanda M.Cuccovia; YanGeng; Emiliano B. Barbarez; Laurence S.Romsted. Proceedings of the 239th ACS National Meeting, Abstracts of Papers, San Francisco, CA, United States, March 21–25, 2010, COLL-133.;
Luis G. Dias, Fabio H. Florenzano, Wayne F. Reed, Mauricio S. Baptista, Silvia M.B. Souza, Emiliano B. Alvarez, Hernan Chaimovich, Iolanda M. Cuccovia, Carmen L. Amaral, Carlos R. Brasil, Laurence S. Romsted, Mario J. Politi, Langmuir 18 (2002) 319.
[6] Davi D.Pavanelli, Properties of giant unilamellar vesicles (Ph.D. thesis), Biochemistry Depto, Institute of Chemistry University of Sao Paulo, 2006.
[7] Miglena I. Angelova, Dimiter S. Dimitrov, Faraday Discuss. Chem. Soc. 81 (1986) 303;
Dimiter S. Dimitrov, Miglena I. Angelova, Prog. Colloid Polym. Sci. 73 (1987) 48;
Miglena I. Angelova, Dimiter S. Dimitrov, Prog. Colloid Polym. Sci. 76 (1988) 59;
Fredric M. Menger, Miglena I. Anglevoa, Acc. Chem. Res. 31 (1988) 789.
[8] Kenichi Nakashima, Kazuki Yuda, Yukihiro Ozaki, Isao Noda, Spetrochim. Acta Part A 60 (2004) 1783;
H. Toyodome, Y. Higo, R. Sasai, J. Kurawaki, Y. Kaneko, J. Nanosci. Nanotechnol. 12 (2013) 3074.
[9] Tatsuto Yul, Tatsuya Kameyama, Takyosi Sasaki, Tsukasa Torimotot, Katsuhiko Takagi, J. Phorphyrins Phthalocyanines 11 (2007) 428;
Pedro M.R. Paulo, César A.T. Laia, Silvia M.B. Costa, J. Phys. Chem. B 107 (2003) 1097;
I.M. Pritula, N. Bezkronav, V. Lopin, M.I. Kolybaeva, V.M. Puzikov, R.I. Zubatyuk, V. Shishkin, V.Ya gayvoronsky, J. Phys. Chem. Solids 74 (2013) 452.
[10] Edward M. Kosower, John L. Cotter, J. Am. Chem. Soc. 86 (1964) 5524.
[11] Detlef W. Bahnemann, Christian-Herbert Fischer, Eberhard Janata, Arnim Henglein, J. Chem. Soc. Faraday Trans. I 83 (1987) 2559.
[12] Bo-Long Poh, Cbi Uing Tan, Chin Line Lob, Tetrahedron 49 (1993) 3849.
[13] K.E. Connors, Binding Constants, Wiley-Interscience, USA, 1987.
[14] M.J. Frisch, G.W. Trucks, H.B. Schlegel, G.E. Scuseria, M.A. Robb, J.R. Cheeseman, J.A. Montgomery , T. Vreven, K.N. Kudin, J.C. Burant, J.M. Millam, S.S. Iyengar, J. Tomasi, V. Barone, B. Mennucci, M. Cossi, G. Scalmani, N. Rega, G.A. Petersson, H. Nakatsuji, M. Hada, M. Ehara, K. Toyota, R. Fukuda, J. Hasegawa, M. Ishida, T. Nakajima, Y. Honda, O. Kitao, H. Nakai, M. Klene, X. Li, J.E. Knox, H.P. Hratchian, J.B. Cross, V. Bakken, C. Adamo, J. Jaramillo, R. Gomperts, R.E. Stratmann, O. Yazyev, A.J. Austin, R. Cammi, C. Pomelli, J.W. Ochterski, P.Y. Ayala, K. Morokuma, G.A. Voth, P. Salvador, J.J. Dannenberg, V.G. Zakrzewski, S. Dapprich, A.D. Daniels, M.C. Strain, O. Farkas, D.K. Malick, A.D. Rabuck, K. Raghavachari, J.B. Foresman, J.V. Ortiz, Q. Cui, A.G. Baboul, S. Clifford, J. Cioslowski, B.B. Stefanov, G. Liu, A. Liashenko, P. Piskorz, I. Komaromi, R.L. Martin, D.J. Fox, T. Keith, M.A. Al-Laham, C.Y. Peng, A. Nanayakkara, M. Challacombe, P.M.W. Gill, B. Johnson, W. Chen, M.W. Wong, C. Gonzalez, J.A. Pople, Gaussian, Inc., Wallingford, CT, 2009.
[15] Walter Kohn, Lou Sham, J. Phys. Rev. A 140 (1965) 1133.
[16] Chengteh Lee, Weitao Yang, Robert G. Parr, Phys. Rev. B 37 (1988) 785.
[17] Axel D. Becke, J. Chem. Phys. 98 (1993) 5648.
[18] Paul C. Hariharan, John A. Pople, Theor. Chim. Acta 28 (1973) 213.
[19] Maurizio Cossi, Giovanni Scalmani, Nadia Rega, Vincenzo Barone, J. Chem. Phys. 117 (2002) 43.
[20] Stefan Dapprich, Gernot Frenking, J. Phys. Chem. 99 (1995) 9352.
[21] Yizhak Marcus, Glenn Hefter, Chem. Rev. 106 (2006) 4585;
R. Breslow, Acc. Chem. Res. 24 (1990) 159;
R. Breslow, C.J. Rizzo, J. Am. Chem. Soc. 113 (1991) 4340.
[22] Hernan G. Chaimovich, João B.S. Bonilha, Mario J. Politi, Frank H. Quina, J. Phys. Chem. 83 (1979) 1851.

[23] S.M.B. Souza, M.B. Silvia, Emiliano B. Alvarez, Mario J. Politi, Recent Trends in Surface and Colloid Science, 12, World Scientific Publishing, Singapore, (2012) 155.
[24] Motohiro Shima, Yohei Kobayashi, Takao Fujii, Miyono Tanaka, Yukitaka Kimura, Shuji Adachi, Ryuichi Matsuno, Food Hydrocolloids 18 (2004) 61;
Alexander B. Artyukhin, Olgica Bakajin, Pieter Stroeve, Aleksandr Noy, Langmuir 20 (2004) 1442;
Shuji Adachia, Hanaho Imaokaa, Hiroko Ashidab, Hirokazu Maedab, Ryuichi Matsunoa, Eur. J. Lipid Sci. Technol. 106 (2004) 225.
[25] Chiho Hamai, Paul S. Cremer, Siegfried M. Musser, Biophys. J. 92 (2007) 1988.